Proceedings of the ASME 2017 International Design Engineering Technical Conferences and Computers and Information in Engineering Conference
IDETC/CIE 2017
August 6-9, 2017, Cleveland, Ohio, USA

DETC2017-67377

DESIGN AND ANALYSIS OF A REDUCED DEGREE OF FREEDOM MODULAR SNAKE ROBOT

Peter Racioppo
Robotics and Mechatronics Lab
Mechanical Engineering Dept.
Virginia Tech
Blacksburg, VA, USA
rpeter8@vt.edu

Wael Saab
Robotics and Mechatronics Lab
Mechanical Engineering Dept.
Virginia Tech
Blacksburg, VA, USA
waelsaab@vt.edu

Pinhas Ben-Tzvi
Robotics and Mechatronics Lab
Mechanical Engineering Dept.
Virginia Tech
Blacksburg, VA, USA
bentzvi@vt.edu

ABSTRACT

This paper presents the design and analysis of an underactuated, cable driven mechanism for use in a modular robotic snake. The proposed mechanism is composed of a chain of rigid links that rotate on parallel revolute joints and are actuated by antagonistic cable pairs and a multi-radius pulley. This design aims to minimize the cross sectional area of cable actuated robotic snakes and eliminate undesirable nonlinearities in cable displacements. A distinctive feature of this underactuated mechanism is that it allows planar serpentine locomotion to be accomplished with only two modular units, improving the snake's ability to conform to desired curvature profiles and minimizing the control complexity involved in snake locomotion. First, the detailed mechanism and cable routing scheme are presented, after which the kinematics and dynamics of the system are derived and a comparative analysis of cable routing schemes is performed, to assist with design synthesis and control. The moment of inertia of the mechanism is modeled, for future use in the implementation of three-dimensional modes of snake motion. Finally, a planar locomotion strategy for snake robots is devised, demonstrated in simulation, and compared with previous studies.

1. INTRODUCTION

Snake robots have been a subject of great interest in the robotics community due to their potential to more easily navigate in cluttered or confined environments than traditional vehicles [1],[2]. Snake robots, like their biological counterparts, are comprised of serially linked segments, and locomote primarily by exploiting anisotropic frictional contact with their environment to produce propulsive forces [3]. The lateral undulation gait, more commonly referred to as serpentine or slithering motion, allows a snake robot to achieve forward movement by propagating sinusoidal waves from head to tail. A condition for this motion is that the robot must make greater frictional contact normal to its body length than along its body length [1],[4]. The strength of such full-body locomotion strategies, which are employed in nature by a diverse array of marine and land animals, is that any part of the robot's body may be used for locomotion [3],[5]. In comparison to wheeled or legged robots, the ability of snake-like mechanisms to engage any of their degrees of freedom (DOFs) in this "hyperredundant" fashion provides them with significant advantages in irregular terrain [6]. However, the large number of DOFs involved in locomotion also considerably complicates control [7].

The majority of the snake robots in the literature consist of serially chained, rigid links, with each joint angle actuated separately [8], [9], [10]. With fewer joints per length than their biological counterparts, these robotic snakes must drive their joint angles at greater amplitude in order to approximate the same curvature profile as a biological snake of equal length. Such designs increase link mass and cross sectional area and require sophisticated motor control [11]. To address these issues, we propose a single degree-of-freedom, modular bending mechanism, which may be substituted in a snake robot in place of straight links. Each module is composed of four rigid links, whose relative angles are controlled by a multi-radius pulley so that the mechanism approximates a standing sinusoidal wave. Locomotion and turning may thus be achieved with only two, single-DOF modules, while the loss of redundancy can be compensated for by passively conforming to

Copyright © 2017 ASME

obstacles with elastic elements, resulting in simplifications to both design and control.

The work described in this paper is part of ongoing research on cable-actuated mechanisms with serpentine [12],[13] and continuum [14]–[18] structures, for use in robotic tails and snakes. This paper presents the design and analysis of the Planar Bender mechanism for use in a reduced-DOF, modular snake robot and is organized as follows: Section 2 provides a review of previous empirical investigations of snake locomotion and robotic snake designs. Section 3 presents the mechanical design and cable-routing method of the bending mechanism. Section 4 presents kinematic and dynamic analyses and explores cable routing schemes. Section 5 presents a preliminary locomotion strategy and its relation to prior snake-robot control schemes. Remarks and plans for future work are discussed in Section 6.

2. BACKGROUND AND DESIGN MOTIVATION

This section provides an overview of prior research into the design of snake-like mechanisms, and empirical studies of locomotion in biological snakes. Essential properties of snake robots are described, including friction characteristics, types of hyperredundant structures, the use of direct-drive versus cable-actuated systems, and compliance. The design motivation for the bending mechanism and general requirements for its operation are then discussed.

2.1 Snake Robots

Early observational studies of serpentine motion in snakes, such as those of W. Mosauer and J. Gray, provided foundational insight into the basic mechanism by which ground friction in the transverse and lateral directions of a snake's body propels it forward, and the importance of the snake's curvature profile for locomotion [19],[5]. Curvature in biological snakes is controlled by an intricately arranged web of axial muscles, which, as shown by J. Gasc, produce angular displacements between adjacent vertebrae in the range of 10 to 20 degrees [20]. Significant angular displacements in biological snakes thus must involve underactuated groups of vertebrae.

Work on snake robots was initiated by S. Hirose's development of ACM III, which demonstrated serpentine motion on a flat plane [21]. Hirose's design employed passive wheels to produce the anisotropic ground friction characteristics necessary for forward locomotion. Passive wheels are a common means of producing anisotropic ground friction in snake robots, but may fail to make effective contact in cluttered or irregular environments. In biological snakes, anisotropic friction is instead produced by the geometrical and mechanical properties of scales [22]. B. Jayne studied the mechanical properties of the skins of six snake species and noted correlations between skin characteristics and locomotion style [23]. Marvi et al., studied active control of scales in corn snakes and developed the two-link inchworm robot ScalyBot, to study the effects of actively adjusted scales on locomotion, on flat and inclined planes [24]. Grooves, static scales, and friction skins have also been widely used to incorporate the desired friction characteristics directly into the construction of a snake robot's outer shell, as in the 3D printed scales employed by the Scaled Snake Robot, or the bristle-covered fabric used in the MMIR robot [25],[26].

The cyclical curving motion executed during serpentine motion may be achieved mechanically using either serpentine or continuum type mechanisms. Serpentine designs, which are defined by their serial chain of rigid links, may closely approximate continuous curves, provided a sufficient level of articulation, with the benefit of robust sub-structures convenient for housing actuation. Continuum designs, which make use of a compliant backbone to achieve continuous bending, eliminate the need for discrete joints, and are thus well suited to small-scale applications. However, continuum mechanisms exhibit problematic sagging under loading and pose difficulties to conventional means of modeling and sensing. Hybrid approaches include the use of multiple backbones [27], interleaved flexible and rigid links [28], and spherical joints situated around an elastic core [29].

The majority of snake robots in the literature are serpentine type mechanisms and employ direct drive at each link to maximize joint torque and drive stiffness. This design choice is incorporated by a wide variety of snake robots, including the Wheeko robot [7], constructed to investigate serpentine motion on a flat plane; the Kulko robot, designed to investigate interaction with obstacles [7]; the reconfigurable PolyBot [30]; and the ACM R5 [31], which demonstrated locomotion in water with the use of fins mounted on each link. Direct drive is also widely used in snake robots which employ active wheels or treads, such as the ACM-R4 and OmniTread OT-8, respectively [32],[33].

Cable-driven actuation in both serpentine and continuum type robots has primarily been pursued in the context of manipulators, as a means of decreasing mass and cross sectional area requirements by allowing the mechanism's actuators to be located away from the joints they actuate [34]. Ota et al. built and tested a serpentine-type robot consisting of a series of cylindrical links only 11 mm in radius, and actuated by internally routed cables [35]. Ouyang et al. developed a continuum-type robot composed of a three-segment, super-elastic nitinol rod backbone with concentric discs used for cable routing [27]. Cable actuation schemes allowed these robots to be small and highly articulated, but required the use of multiple externally driven pulleys.

In self-contained mechanisms, where space is limited, the use of cabling requires that pulley and actuation systems be made as compact as possible. Antagonistic cable pairs and multi-radius pulleys may be used in this context to consolidate the actuation of multiple links. A variety of mechanisms which use antagonistic pairs of cables to generate joint motion have been designed, including Hillbery and Rolamite joints, which employ cylindrical rollers actuated by antagonistic bands to produce low-friction, planar bending [36]. A number of cable actuated robotic hand designs have incorporated antagonistic

Copyright © 2017 ASME

cable pairs, including the DLR, a versatile, variable stiffness robotic hand, and the PISA/IIT SoftHand, which exploits underactuated, compliant cabling to produce adaptive grasping behavior [37],[36]. A disadvantage of straight-line routing of antagonistic cables in bending mechanisms is that displacements in antagonistic cable segments may exhibit nonlinearities during bending, depending on the details of the routing scheme. This challenge is discussed in more detail in Section 4.

Compliant elements may be included in snake robots to filter high frequency disturbances, shield motors, and enable automatic conformation to obstacles, highly desirable properties for robots that engage their entire bodies during locomotion [38], [39]. Rollinson et al. developed a snake robot that employed series elastic actuators (SEAs) consisting of conical rubber elements placed at each joint, and demonstrated three-dimensional gaits and climbing of vertical poles [40]. Ahmed and Billah designed a compliant backbone snake robot incorporating flexible tendons made from electroactive polymer materials [41].

2.2 Design Motivation

Lessons derived from the literature highlight several main factors that drove the design of the Planar Bender mechanism.

- Biological snakes display small maximum angular displacements between adjacent links and continuous curvature during lateral undulation. Groups of links can thus be approximated with underactuated, curving structures
- Snake robots are typically actuated with bulky, direct-drive motors. Actuating multiple links with a single motor via cabling allows link mass and cross sectional area to be reduced and avoids the problems associated with direct drive.
- Cable-driven serpentine mechanisms are often limited by the size of pulley actuation systems, which may be made smaller using antagonistic cable pairs and multi-radius pulleys.
- Straight routing schemes may produce nonlinearities in the displacement of antagonistic cable pairs. This problem can be avoided by routing cables along circular surfaces.

3. MECHANICAL DESIGN

This section describes the mechanical design of the Planar Bender, shown in Fig. 1, and the mechanism's cable-routing scheme.

Each bender is a modular, single-DOF unit, composed of a serial chain of N rigid links connected by parallel revolute joints. The mechanism is actuated by an antagonist-pair tendon transmission system, in which opposing cables coordinate their contraction and elongation phases to avoid interfering with each other's motion. The N–1 cable pairs are routed along the circular exteriors of the links in circular grooves, which prevent lateral slippage and cable interference. Routing cables along circular paths rather than routing in straight lines from link to link constrains the cable displacements on opposite sides of the mechanism to be equal and opposite in value, as will be further

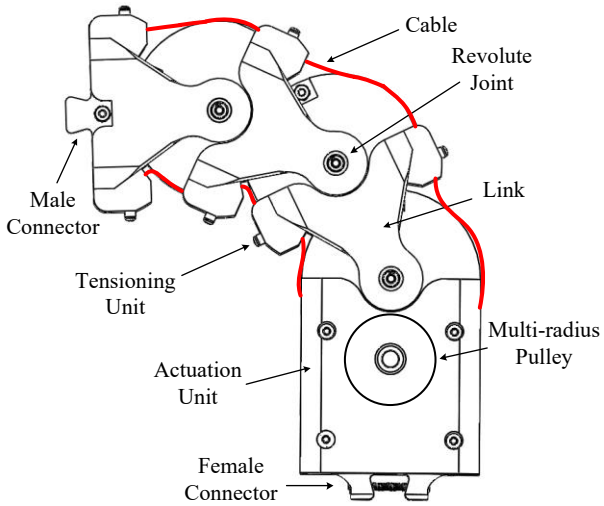

FIG. 1. DESIGN OF THE PLANAR BENDER

discussed in Section 4. Each cable pair attaches to a single link and terminates on a multi-radius pulley, located in the actuation unit. Rotating the pulley displaces each cable segment, inducing a curvature profile in the mechanism that depends on the ratios of the pulley radii. The cable pair that connects to the nth link is routed along all of the n–1 intermediate links, resulting in kinematic coupling, since the cable displacement that occurs at the nth link is influenced by the rotation of those between it and the base. The pulley is driven with a high-torque servomotor, which is inserted into the base compartment via a detachable side-wall, to ensure proper alignment of the pulley channels with the exterior cable grooves. Given the pulley radii, a single rotary encoder on the servomotor shaft is sufficient to determine the full bending profile of the mechanism. Each of the driven links is hollow and low mass, providing extra space for electronics and on-board batteries.

Cable tensioning, which is necessary to prevent backlash and hysteresis-nonlinearities, and ensure that the mechanism is in a straight configuration at equilibrium, is accomplished using a sliding tensioning unit, which inserts into slots in laterally placed bars on the side of each link. Tightening screws on a tensioning unit forces it further into its slot, increasing the tension on the wires that pass underneath. These units also prevent cables from slipping normal to the link surfaces. Tensioning must be performed sequentially, starting with the link closest to the base, in order to ensure that the kinematic constraints consistent with a straight configuration are satisfied at each step.

Compliance is of particular importance in the context of a reduced-DOF snake, as it allows the robot to automatically conform and rebound from obstacles in the absence of individually actuated joints. Elastic elements also perform the vital task of filtering the high-frequency disturbances that arise during locomotion, which decreases the shock impulses experienced by the motor. Compliance in the Planar Bender is

Copyright © 2017 ASME

achieved with extension springs attached in series with each of the cables, removing the need for a specially designed torsional element, which would increase the size of the base compartment. Cable lengths at the home configuration are selected to produce a small extension in each of the springs, such that all of the springs remain in tension throughout bending.

The anisotropic friction characteristics necessary for locomotion are produced using a bristle-covered fabric whose friction characteristic depend on the orientation of the bristles relative to the ground plane. This friction-skin material produces different coefficients of friction in its lateral and transverse orientations, defined relative to the alignment of the bristles, and has already been characterized by the authors in the context of inchworm locomotion [26]. The small-scale structure of the friction skin is well suited to producing anisotropic friction on regular and even terrain, such as carpeted or tiled surfaces. During planar movement, the rigid structure of the bender ensures that every part of the friction skin is on a level plane and remains uniformly engaged. The skin has the property that the coefficient of friction that opposes forward motion is lower than the corresponding coefficients for both backward and lateral motion. The combination of these two properties is ideal for producing forward locomotion, as it both supports the serpentine gait and prevents back-slipping.

The Planar Bender is designed to be a self-contained experimental platform for investigating a variety of modes of snake locomotion. To that end, each module includes a male-female interface as a simple means of connecting modules in series, while the curvature profile of the mechanism may be modified at any time by replacing the pulley. Connecting multiple Planar Benders in series produces a "Planar Slitherer," displayed in Figure 2, two modules being the minimum required for serpentine locomotion and turning. Modifying the curvature of each Planar Bender sinusoidally and out of phase with the adjacent module produces forward locomotion. Turning may be the maximum angular displacements on the left and right sides are unequal, resulting in a moment which rotates the snake. The ability of each module to independently execute a full bending motion allows for the addition of components with other functions, without the loss of slithering functionality. Modules that enable additional degrees of freedom, such as inchworm-like linear progression or rotation about the snake's principal axis, may be linked in series with bending modules to enable both planar slithering and three-dimensional motion, as shown in Fig. 2.

4. ANALYSIS

This section presents kinematic and dynamic analyses of the Planar Bender in Sec. 4.1 and 4.2, calculations of cable displacements in antagonistic cabling systems with straight wire routing in Sec. 4.3, a discussion of circular wiring schemes in Sec. 4.4, and calculations pertaining to three-dimensional motion in Sec. 4.5.

4.1 Kinematics

The curvature profile of an N-link Planar Bender is defined by its N–1 relative joint angles θ_i, each of which may be written in terms of the angular displacement θ_P of the multi-radius pulley. A simplified, two-link schematic is shown in Fig. 3, where cables are drawn as straight lines for the sake of simplicity. Here, r_i is the radius of the ith pulley section, l_i is the radius of link i, h_i denotes the normal distance between adjacent revolute joints, and D_i is the distance between the ith joint and the point where the cables make contact on the end of the ith link. In the Planar Bender l_i, h_i, and D_i are taken as constant for all i.

To determine the first relative joint angle θ_1, note that a given pulley rotation θ_P causes a displacement of $r_1\theta_P$ in the cable segment attached to the first link, which must equal the arc length subtended by θ_1. The angular displacement of the first link corresponding to a pulley rotation of θ_P is thus

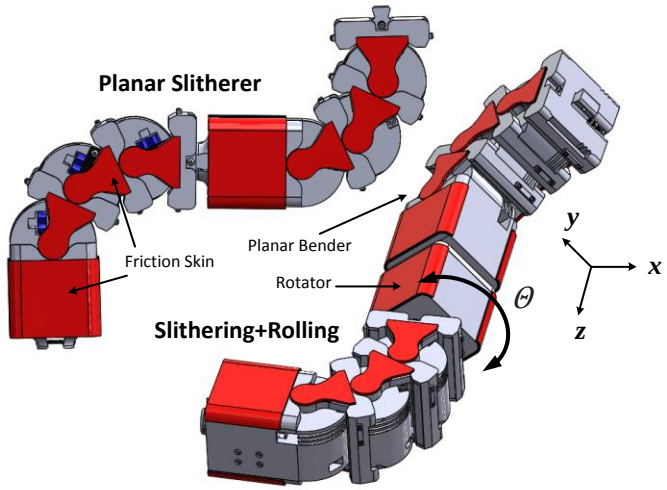

FIG. 2. SNAKE ROBOT DESIGN

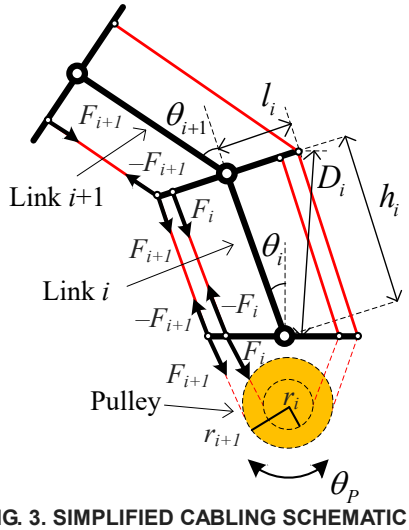

FIG. 3. SIMPLIFIED CABLING SCHEMATIC

Copyright © 2017 ASME

Subsequent joint angles may be calculated recursively by computing the rotation of link i relative to the pulley frame and then subtracting off the contributions to this rotation that come from the i–1 previous links:

$$\theta_i = \frac{r_i}{D_i}\theta_P - \sum_{j=1}^{i-1}\theta_j \tag{1}$$

This expression may be written more compactly by applying the previous argument for general i: $D_i(\theta_{i-1}+\theta_i)/(D_{i-1}\theta_{i-1}) = r_i/r_{i-1}$, which implies that for $i > 1$,

$$\theta_i = \left(\frac{r_i}{D_i} - \frac{r_{i-1}}{D_{i-1}}\right)\theta_P \tag{2}$$

The bending profile of the mechanism may thus be manipulated by appropriate selection of the relative pulley radii. Progressive bending along the mechanism requires a monotonic increase in the corresponding pulley radii: $r_1 < r_2 < \ldots < r_n$, which limits the number of links that the mechanism can accommodate for a given cross sectional area.

4.2 Dynamics

The torques applied on each joint by the application of a motor torque may be calculated by examining the resulting cable tensions. As can be seen in Fig. 3, the tension forces acting on link i, in the cables above and below that link, occur in equal and opposite pairs. For link i, the only cable forces that generate a moment in joint i are the pair acting between links i–1 and i. The relation between motor torque and joint torque is thus given by a system of N equations in N unknowns:

$$\tau_{\mathrm{M}} = \sum_{i=1}^{N-1} F_i r_i \quad , \quad \tau_i = \sum_{j=i}^{N-1} F_j l_j \tag{3}$$

Joint torques can be found from cable tensions by solving (3) recursively from the tip of the mechanism to its base.

4.3 Straight-Line Cable Displacements

Straight cable routing schemes, though advantageous for their simplicity, pose potential problems for antagonistically routed systems due to potential nonlinearities in the sum of the displacements that occur in cable pairs. The present analysis investigates these nonlinearities and means of offsetting them, with reference to the schematic displayed in Fig. 4. Here, the angles α and β are design parameters that define the angles at which the cables connect to the lower portion of the (i+1)th link and the upper portion of the ith link, respectively, in terms of the local coordinate frames of the links.

The lengths of the straight cable sections on the left and ride sides of the ith link are given, respectively, by the norms

$$LS_i = \left\| R_i \left(\begin{bmatrix} 0 \\ h_i \end{bmatrix} - R_\alpha \begin{bmatrix} l_i \\ 0 \end{bmatrix} \right) + R_{i-1} R_{-\beta} \begin{bmatrix} l_i \\ 0 \end{bmatrix} \right\|_2 \tag{4}$$

$$RS_i = \left\| R_i \left(\begin{bmatrix} 0 \\ h_i \end{bmatrix} + R_{-\alpha} \begin{bmatrix} l_i \\ 0 \end{bmatrix} \right) - R_{i-1} R_{\beta} \begin{bmatrix} l_i \\ 0 \end{bmatrix} \right\|_2$$

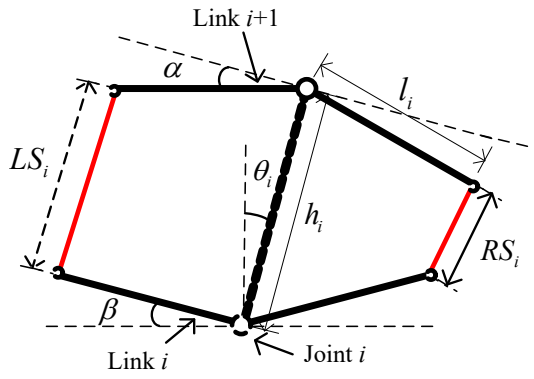

FIG. 4. STRAIGHT WIRING SCHEME

where R_i is the rotation matrix corresponding to the angle θ_i, and R_α and R_β are the rotation matrices for the angles α and β, respectively.

The total change in the length of the nth cable (i.e. the cable that originates on the nth pulley section and terminates on the nth link) required to accommodate a pulley rotation of θ_P is given by the sum of the segment displacements on the two sides:

$$\Delta_n = \Delta_{L,n} + \Delta_{R,n} \tag{5}$$

$$\Delta_{L,n} = \sum_{i=1}^{n}\left(LS_i - LS_{i,0}\right) + r_n\theta_P$$

$$\Delta_{R,n} = \sum_{i=1}^{n}\left(RS_i - RS_{i,0}\right) - r_n\theta_P$$

where $LS_{i,0}$ and $RS_{i,0}$ are the values of LS_i and RS_i when the mechanism is straight (i.e. $\theta_P = 0$).

Since cable length must remain constant, each Δ_n should equal zero for all θ_P. However, as equation (4) shows, Δ_n in a mechanism described by (5) is nonlinear and, in general, nonzero for $\theta_P \neq 0$.

One method of compensating for cable nonlinearities is to place extension springs in series with the cables so that over-extended cables can shift their attachment point to accommodate desired angular displacements. Nonlinearities in cable displacements are thus replaced by nonlinearities in cable tensions, due to the forces exerted by the springs. Namely, a torque $\tau_{Elastic,i} = -k_i l_i \Delta_i$ is exerted on each joint, where k_i is the spring constant of the nth extension spring. These nonlinearities can be approximately canceled out by adding a feedforward control torque. In order to compensate for the elastic torques occurring at each of the N–1 joints, the feedforward torque τ_{FF} must simultaneously satisfy the N–1 conditions:

$$\tau_{\mathrm{FF}} = \sum_{i=1}^{N-1} r_i \left(\frac{k_i \Delta_i r_i}{R_i} - \frac{k_{i+1}\Delta_{i+1} r_{i+1}}{R_{i+1}} \right) \tag{6}$$

Thus, if the ratios of the displacement errors in the cables remain approximately constant, spring constants may be selected according to (6) so that a single control term applied at

Copyright © 2017 ASME

the base motor approximately cancels the torques produced by the nonlinearities in cable displacement, at every joint.

Figure 5(a) plots the total cable displacement in each of the three cables in a four-link mechanism described by (4), as it executes a series of sinusoidal bending motions. Here dimensional parameters were set to: $l_i = 1.5h_i$, with l_i and h_i constant for all i, $r_1 = 0.2h_i$, $r_2 = 1.5r_1$, $r_3 = 2r_1$, $\alpha = 30°$, and $\beta = 10°$, with an input frequency of 1.5 Hz and maximum joint angle of 35°. Figure 5(b) plots the error Δ_n in the length of each cable as a percent of each cable's total length at the mechanism's home configuration. During this motion, Δ_2/Δ_1 and Δ_3/Δ_1 exhibit large nonlinearities as the mechanism approaches a singular configuration (i.e. as $\{\Delta_1, \Delta_2, \Delta_3\} \to 0$).

While (6) provides a means of compensating for cable displacement errors, it is also desirable to understand how these errors can be minimized or avoided by appropriate selection of model parameters. In particular, an understanding of the dependence of cable error on link geometry informs the process of design synthesis. For this purpose, a sensitivity analysis, displayed in Fig. 6, was performed on the percent error in cable displacement in a two-link mechanism with respect to h/l as the mechanism bends, with the first joint angle θ_1 in this case increasing from 0° to 40°.

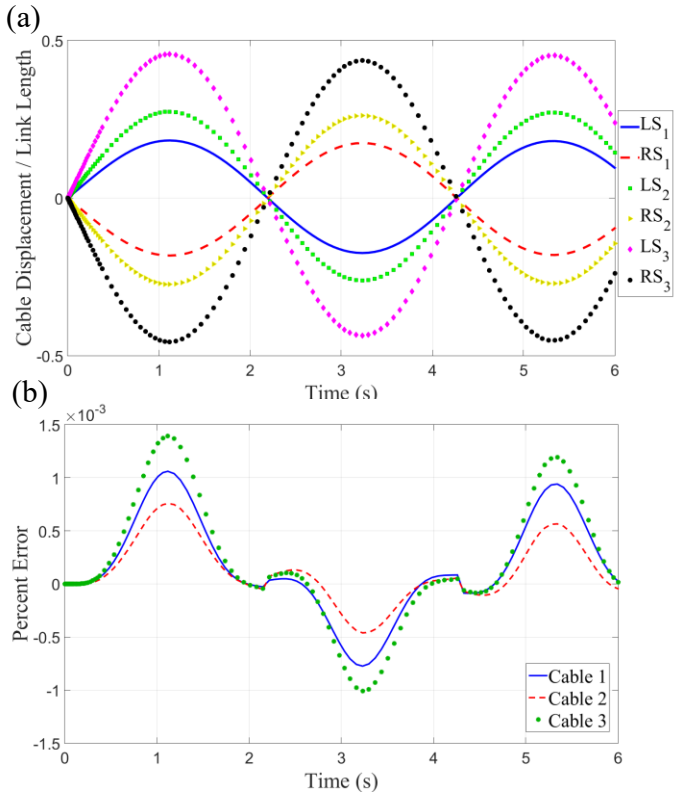

FIG. 5. SIMULATIONS OF CABLE DISPLACEMENT: (a) CABLE DISPLACEMENT / LINK LENGTH, (b) PERCENT ERROR IN CABLE DISPLACEMENT

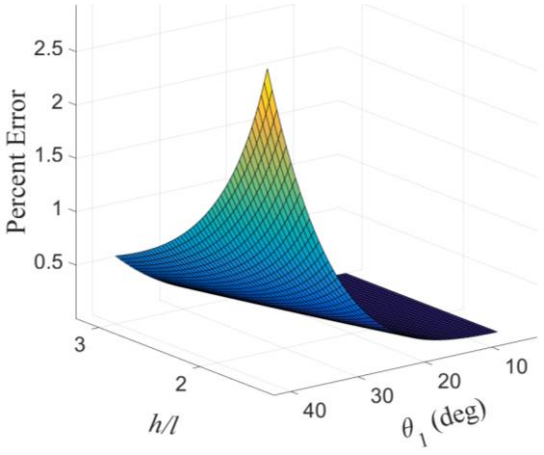

FIG. 6. CABLE DISPLACEMENT ERROR FOR VARYING LINK GEOMETRY

Here, the design parameters α and β are taken to be zero. For large θ_1, cable displacement error can be seen to increase sharply as h/l, the height to width ratio of the links, approaches zero.

4.4 Circular Wiring Scheme

While the nonlinearities that occur in straight cable routing schemes may be offset using the techniques described in Section 4.3, they may be avoided altogether by constraining the cables to follow circular paths. A schematic of the paths taken by cables around a bending mechanism with circular links is shown in Fig. 7. As in Section 4.3, the angle α specifies the last points at which the cables make contact with the lower portions of the links, in terms of the links' local coordinate frames. The points at which the cables contact the upper portion of each link's circular surface are defined for the left and right sides by the angles β_l and β_r. The design parameter η specifies the angle at which each link's circular arc extends beyond the local x-axis, where $\eta = 0°$ for a semicircle and $\eta = 90°$ for a full circle. Unlike in Section 4.3, α and β are variable and may be determined by finding the line which is tangent to both circles for some θ_i. In the case of equal, circular links, (constant l_i) where $\eta \geq 0°$, the line between α and β tracks θ_i and is therefore

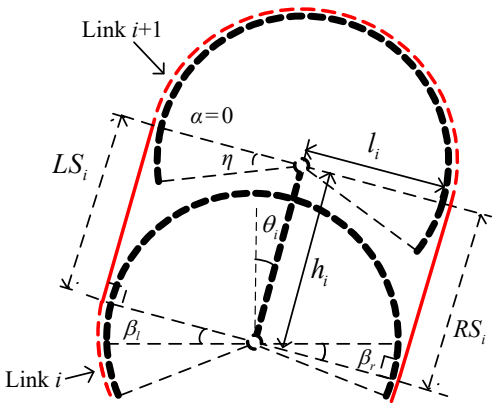

FIG. 7. CIRCULAR WIRING SCHEME

Copyright © 2017 ASME

parallel to the line between circle centers. In this case, $\alpha = 0°$ and $\beta_l = -\beta_r$, so that for $\theta_i \le \eta$, $LS_i = RS_i$ and the total cable length remains constant, that is, $\Delta_n = 0$ for all $n \in \{1, 2, \ldots, N-1\}$. Thus, the design parameter η is equal to the maximum angular displacement that the links can undergo before encountering nonlinearities in cable displacement.

In order to avoid mechanical interference between the circular and straight-line portions of adjacent links, link geometry must satisfy the condition

$$\begin{cases} \eta \le \dfrac{\pi}{2} - \arcsin\left(\dfrac{h}{2l}\right) & \text{for } \dfrac{h}{l} \le \sqrt{2} \\ \dfrac{h}{l} = \sin\eta + \sin\left(\dfrac{\pi}{2} + \eta\right) & \text{for } \dfrac{h}{l} \ge \sqrt{2} \end{cases} \tag{7}$$

A design tradeoff must thus be made between minimizing the total length of the mechanism and maximizing the range of the joint angles over which $\Delta_n = 0$. Nonlinearities that occur when $\theta_i \ge \eta$ may be dealt with by the same means as in Section 4.3, since β will remain fixed at the link's endpoint in this range.

In the Planar Bender, we have chosen to implement the circular wiring scheme described above using circular grooves, and we have chosen $\eta \approx 35°$.

4.5 Three Dimensional Motions

While The rigid structure of each Planar Bender module allows for rotation about the axis which runs along the length of its body (which we call the z-axis) without a change in bending due to coupling or sagging. Thus, a rolling motion of a bender about the z-axis by an angle Θ transforms the local coordinate frame by $R_{z,\Theta}$, the rotation matrix about the z-axis for that angle. The Planar Bender is designed for both planar maneuvers and spatial maneuvers in conjunction with a rotational unit. Including a pure rolling-DOF departs from the biological design, and may allow for the use of gaits not found in nature. A gait similar to sidewinding, where bending sections are progressively lifted and placed down, should also be possible. Performing three-dimensional movements will require precise coordination of the bending-DOF with the rolling-DOF, making it necessary to understand how the dynamics of the bending mechanism, and particularly its moments of inertia, change as it bends.

We define the y-axis as the axis perpendicular to the plane of bending and the z-axis as the one about which the rolling-DOF acts (referring to Fig. 2), and we define $I_{Y,i}$ and $I_{Z,i}$ as the moments of inertia of the ith link about these respective axes. Modeling the links as thin rods, the y-axis moments of inertia may be computed recursively as $I_{Y,i} = m_i\lambda_{i,y}^2 + m_i h_i^2/12$, where $\lambda_{i,y} = [\Lambda_{i-1}^2 + (h_i/2)^2 - \Lambda_{i-1}h_i\cos(\psi_{i-1})]^{1/2}$ is the distance from the origin to the ith link center and $\Lambda_i = [\Lambda_{i-1}^2 + h_i^2 - 2\Lambda_{i-1}h_i\cos(\psi_{i-1})]^{1/2}$ is the distance from the origin to the ith joint. We define the angle $\psi_i = \theta_i - \alpha_i$, where $\alpha_i = \arcsin[(h_{i-1}/\Lambda_i)\sin(\psi_{i-1})]$, and $\psi_1 = \theta_1$. The z-axis moment of inertia may be modeled by treating each of the links as a solid cylinder of radius l_i, height h_i, and mass M_i. Employing moment of inertia tensor transformations, $I_{Z,i} = \frac{1}{2}(I_{z,i} + I_{x,i}) + \frac{1}{2}(I_{z,i} - I_{x,i})\cos(2\theta_i)$, where $I_{z,i} = \frac{1}{2}M_i l_i^2$ is the moment of inertia of each cylinder about its axis and $I_{x,i} = (M_i/h_i)[l_i^2(h_i - \lambda_{i,z})/4 + (h_i - \lambda_{i,z})^3/3]$ is the moment of inertia of each cylinder about a line normal to its surface and passing through its base. Here, $I_{x,i}$ is given by the relation $\lambda_{i,z} = \Sigma_{k=2}^{i}|h_{k-1}\sin(\theta_{k-1})|$.

The above expressions for I_y and I_z were computed numerically, where M_i, h_i, l_i, and θ_i were taken to be constant for all i. Figure 8 displays the results of these calculations, normalized by the moments of inertia of the first link, as the angle of the first joint moves from –60° to 60°.

5. SNAKE LOCOMOTION

This section presents an overview of serpentine motion in snake robots that actuate every joint individually, and applies these principles to devise a locomotion strategy for a snake robot composed of underactuated bending mechanisms.

A discrete approximation to the sinusoidal shape of a biological snake undergoing planar lateral undulation, for a snake robot with N equal, straight links is given in terms of the snake's $i \in \{1, \ldots, N-1\}$ joint angles by the expression

$$\theta_{\text{ref},i} = \alpha\sin(\omega t + (i-1)\delta) + \phi_0 \tag{8}$$

where α and ω are the amplitude and angular frequency of the angular displacement, respectively, δ is the phase offset between adjacent joints, and ϕ_0 is a parameter which induces turning for nonzero values, assumed here to be constant [7]. Serpentine motion with constant α, ω, and ϕ_0 (i.e. constant turning radius and speed) may thus be parameterized by a single variable, and is therefore a single degree-of-freedom motion, with an additional degree of freedom sufficient to parameterize planar turning.

As shown by Liljebäck, et al., the $\delta(N)$ that maximizes the average forward velocity of a snake robot driving its joint angles according to (8), under the assumptions of equal link lengths and no side-slipping, is equal to the $\delta(N)$ that maximizes k_δ, where

$$k_\delta = \sum_{i=1}^{N-1}\sum_{j=1}^{N-1} a_{ij}\sin\big((j-i)\delta(N)\big) \tag{9}$$

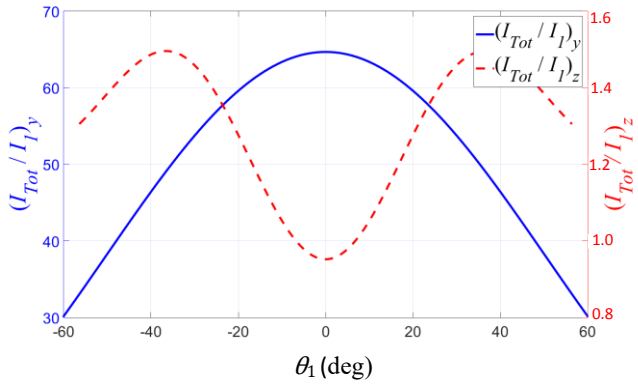

FIG. 8. MOMENTS OF INERTIA

Copyright © 2017 ASME

and where a_{ij} is the ijth element of the matrix $\mathbf{A}\bar{\mathbf{D}} \in \mathbb{R}^{(N-1)\times(N-1)}$, given in [7]. In the case $N = 3$, numerical solution of (9) shows that the optimal phase offset is $\delta = \pi/2$, so that the first and last link of the three-link snake robot are 180° out of phase. The two halves of the snake thus take turns producing moments about the center of mass, so that the robot traces out a sinusoidal-like trajectory. The observation of this behavior in a 3-link snake suggests that it may be the generally applied strategy to maximize forward velocity, in which case a closed form approximation for (9) would be given by the expression

$$\delta = \frac{\pi}{N-1} \tag{10}$$

A comparison of the numerical result given by (9) and the closed form expression in (10) is presented in Fig. 9, for N between 0 and 30 links. The two expressions are in close agreement, with (9) undergoing a higher order oscillation about (10), according to the parity of N.

By analogy with the control strategy for a 3-link snake robot that is actuated at each link, a snake composed of two Planar Benders may achieve locomotion by driving each module to approximate a half-period of a sinusoid, at some phase offset from each other. In the case of equal link lengths, (10) may be used to determine the optimal curvature profile of an N-link Planar Bender at maximum amplitude. To determine the optimal phase offset between m Planar Benders of n links each, note that each link of a bender must be driven at a phase difference of $d = (n-1)\delta$ with respect to the corresponding link in the adjacent bender. Applying (10) with $N = mn-(m-1)$, since the links that connect modules have zero relative angle, gives a phase difference between adjacent modules of $d \approx \pi/m$.

In the case of unequal link lengths, due to the presence of the actuation module in one of the links, we can obtain desired maximum angular displacements by fitting the discrete snake to a sine wave of amplitude A. Treating each link as a point located at its center of mass, the problem of fitting the mechanism to $A\sin(x)$ reduces to a least squares fit of N points to the sine wave. The optimized joint angles obtained by this procedure may then be used with equation (2) to determine the optimized pulley radius ratios.

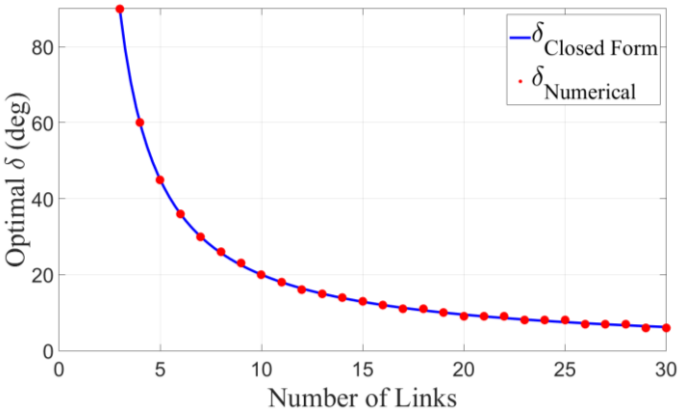

FIG. 9. OPTIMAL PHASE OFFSET VS NO. OF LINKS

Locomotion in a snake robot composed of i benders may be achieved by applying a control torque at each motor of

$$\tau_{\mathrm{M},i} = k_P\left(\theta_{\mathrm{ref},i} - \sum_{j=1}^{N-1}\theta_{i,j}\right) + k_D\left(\dot{\theta}_{\mathrm{ref},i} - \sum_{j=1}^{N-1}\dot{\theta}_{i,j}\right) \tag{11}$$

where k_P and k_D are proportional and derivative gains, $\theta_{i,j}$ is the jth joint angle of the ith bender, and $\theta_{\mathrm{ref},i}$ is given by (8).

The controller in (11) was demonstrated in a dynamic simulation of serpentine locomotion and turning in a two-bender snake robot. Each bending mechanism was represented as a serial chain of straight links connected by revolute joints and obeying the kinematic constraints specified by (2), with exterior frictional forces taken to be viscous. The sums of the joint angles in the two benders and corresponding motor torques are displayed in Fig. 10, for 70 seconds of snake locomotion. In the simulation in Fig. 10, the snake robot has a total mass of 1.4 kg, pulley radii of r_1 = 6 cm, r_2 = 11 cm, and r_3 = 16 cm, l_i = 35 cm for all links, and frictional coefficients of c_t = 0 and c_l = 1 in the transverse and lateral directions, respectively. The control parameters are set at $\alpha = 1$ rad, $\omega = 2$ Hz, and d = 1.5 rad, with a maximum motor torque of 0.1 Nm. The snake is made to travel in a straight line between $t = 0$ s and t = 10 s, turn 135° clockwise between t = 10 s and t = 30 s,

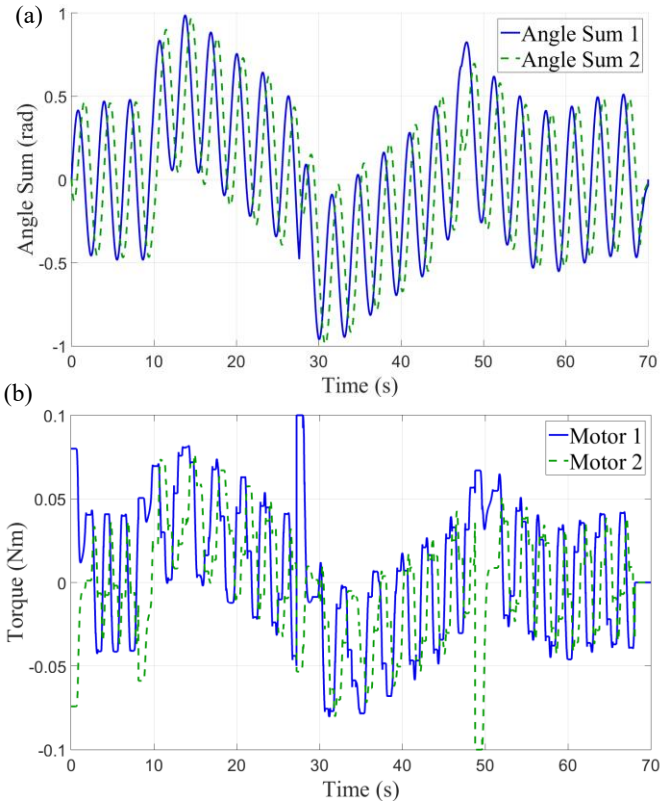

FIG. 10. SIMULATION OF SNAKE LOCOMOTION: (a) SUM OF JOINT ANGULAR DISPLACEMENTS, (b) MOTOR TORQUES

Copyright © 2017 ASME

turn 90° counterclockwise between $t = 30$ s and $t = 50$ s, and then resume straight travel between $t = 50$ s and $t = 70$ s. The intervals of turning may be identified in Fig. 10 as those periods of time during which the angle sums integrate to nonzero values. During its 70 s of travel, the snake robot moved a total distance of approximately 9.3 m. The maximum steady velocity in simulation occurred at $d \approx 0.7$ rad, about 45% lower than the prediction given by Eq. (10). This discrepancy is likely due to the presence of side-slipping and details of link geometry.

6. CONCLUSION

This paper presented the design and analysis of a cable-actuated, single-DOF bending mechanism, for use in robotic snakes. Cables were routed in agonist-antagonist pairs and actuated by a multi-radius pulley, in order to minimize the robot's mass and cross-sectional area. Nonlinearities in cable displacement were avoided by routing the cables along the exterior of circular links. Relative pulley radii determined the curvature profile of the mechanism, which was made to approximate a sinusoidal shape ideal for planar serpentine locomotion. One disadvantage of a circular cabling scheme that should be addressed in future work is that large cable lengths must make contact with link surfaces, increasing frictional losses in transmission efficiency. Minimizing frictional losses in designs of this type is a goal of future study.

Future work will involve further development of a dynamic model to refine design parameters and test control strategies for snake locomotion. Dynamic modeling will be used to compare serpentine locomotion in snakes that employ reduced-DOF elements to that of snakes that independently actuate every joint angle. Experimentation with a finalized prototype will then be performed to validate simulated results and refine the controller. The use of modules designed to allow translational and rotational motion will also be further explored, along with their use in three-dimensional gaits.

REFERENCES

[1] S. Hirose, "Biologically Inspired Robots (Snake-like Locomotors and Manipulators)," *Oxford Univ. Press*, 1987.

[2] P. Liljebäck, K. Y. Pettersen, Ø. Stavdahl, and J. T. Gravdahl, "Snake robot locomotion in environments with obstacles," *IEEE/ASME Trans. Mechatronics*, vol. 17, no. 6, pp. 1158–1169, 2012.

[3] D. L. Hu, J. Nirody, T. Scott, and M. J. Shelley, "The mechanics of slithering locomotion.," *Proc. Natl. Acad. Sci. U. S. A.*, vol. 106, no. 25, pp. 10081–10085, 2009.

[4] P. Liljebäck, K. Y. Pettersen, Ø. Stavdahl, and J. T. Gravdahl, "Controllability and stability analysis of planar snake robot locomotion," *IEEE Trans. Automat. Contr.*, vol. 56, no. 6, pp. 1365–1380, 2011.

[5] J. Gray, "The Mechanism of Locomotion in Snakes," *J. Exp. Biol.*, vol. 23, no. 2, 1946.

[6] A. A. Transeth and K. Y. Pettersen, "Developments in snake robot modeling and locomotion," *9th Int. Conf. Control. Autom. Robot. Vision, 2006, ICARCV '06*, 2006.

[7] P. Liljebäck, K. Y. Pettersen, Ø. Stavdahl, and J. T. Gravdahl, *Snake Robots*. 2013.

[8] S. K. Gupta, A. K. Priyadarshi, S. K. Gupta, R. Gouker, F. Krebs, and M. Shroeder, "A survey of snake-inspired robot designs," *Bioinspiration and Biomimetics*, 2009.

[9] P. Liljebck, K. Y. Pettersen, Ø. Stavdahl, and J. T. Gravdahl, "A review on modelling, implementation, and control of snake robots," *Rob. Auton. Syst.*, vol. 60, no. 1, pp. 29–40, 2012.

[10] D. Rollinson, "Control and Design of Snake Robots," *Dissertations*, no. June, 2014.

[11] D. Vischer and O. Khatib, "Design and Development of Torque Controlled Joints," *Experimental Robotics I*. 1990.

[12] W. S. Rone and P. Ben-Tzvi, "Static modeling of a multi-segment serpentine robotic tail," *ASME 2015 Int. Des. Eng. Tech. Conf. Comput. Inf. Eng. Conf.*, 2015.

[13] W. Saab and P. Ben-Tzvi, "Design and Analysis of a Discrete Modular Serpentine Robotic Tail for Improved Performance of Mobile Robots," *ASME 2016 Int. Des. Eng. Tech. Conf. Comput. Inf. Eng. Conf.*, 2016.

[14] W. S. Rone and P. Ben-Tzvi, "Continuum robot dynamics utilizing the principle of virtual power," *IEEE Trans. Robot.*, vol. 30, no. 1, pp. 275–287, 2014.

[15] W. S. Rone and P. Ben-Tzvi, "Continuum Manipulator Statics Based on the Principle of Virtual Work," *ASME 2012 Int. Mech. Eng. Congr. Expo.*, 2012.

[16] W. S. Rone and P. Ben-Tzvi, "Mechanics Modeling of Multisegment Rod-Driven Continuum Robots," *J. Mech. Robot.*, vol. 6, no. 4, p. 41006, 2014.

[17] W. S. Rone and P. Ben-Tzvi, "Multi-segment continuum robot shape estimation using passive cable displacement," *ROSE 2013 - 2013 IEEE Int. Symp. Robot. Sensors Environ. Proc.*, no. 1334227, pp. 37–42, 2013.

[18] W. S. Rone and P. Ben-Tzvi, "Continuum Robotic Tail Loading Analysis for Mobile Robot Stabilization and Maneuvering," *ASME 2014 Int. Des. Eng. Tech. Conf. Comput. Inf. Eng. Conf.*, 2014.

[19] W. Mosauer, "On the locomotion of snakes," *Science (80-.).*, no. 76, pp. 583–585, 1932.

[20] J. Gasc, "Axial musculature," *Biol. Reptil.*, vol. 11, 1981.

[21] M. Mori and S. Hirose, "Development of active cord mechanism ACM-R3 with agile 3D mobility," *Proc. IEEE/RSJ Int. Conf. Intell. Robot. Syst.*, vol. 3, pp. 1552–1557, 2001.

[22] M. J. Baum, A. E. Kovalev, J. Michels, and S. N. Gorb, "Anisotropic friction of the ventral scales in the snake lampropeltis getula californiae," *Tribol. Lett.*, vol. 54, no. 2, pp. 139–150, 2014.

[23] B. C. Jayne, "Mechanical behaviour of snake skin," *J. Zool.*, vol. 214, no. 1, pp. 125–140, 1988.

[24] H. Marvi, G. Meyers, G. Russell, and D. L. Hu, "Scalybot: A snake-inspired robot with active control of friction," *ASME 2011 Dyn. Syst. Control Conf. Bath/ASME Symp. Fluid Power Motion Control. DSCC 2011*, vol. 2, pp. 443–450, 2011.

[25] M. M. Serrano, A. H. Chang, G. Zhang, and P. A. Vela, "Incorporating frictional anisotropy in the design of a robotic snake through the exploitation of scales," *Proc. - IEEE Int. Conf. Robot. Autom.*, vol. 2015–June, no. June, pp. 3729–3734, 2015.

[26] W. Saab, A. Kumar, and P. Ben-Tzvi, "Design and Analysis of a Miniature Modular Inchworm Robot," *ASME 2016 Int. Des. Eng. Tech. Conf. Comput. Inf. Eng. Conf.*, p. DETC2016-59386, 2016.

[27] B. Ouyang, Y. Liu, and D. Sun, "Design of a three-segment continuum robot for minimally invasive surgery," *Robot. Biomimetics*, vol. 3, no. 1, pp. 1–4, 2016.

[28] B. L. Conrad, J. Jung, R. S. Penning, and M. R. Zinn,

Copyright © 2017 ASME

"Interleaved continuum-rigid manipulation: An augmented approach for robotic minimally-invasive flexible catheter-based procedures," *Proc. - IEEE Int. Conf. Robot. Autom.*, pp. 718–724, 2013.

[29] Z. Li and R. Du, "Design and analysis of a bio-inspired wire-driven multi-section flexible robot: Regular paper," *Int. J. Adv. Robot. Syst.*, vol. 10, 2013.

[30] M. Yim, D. G. Duff, and K. D. Roufas, "PolyBot: a modular reconfigurable robot," *Proceedings 2000 ICRA. Millennium Conference. IEEE International Conference on Robotics and Automation. Symposia Proceedings (Cat. No.00CH37065)*, vol. 1. pp. 514–520, 2000.

[31] H. Yamada, S. Chigisaki, M. Mori, K. Takita, K. Ogami, and S. Hirose, "Development of amphibious snake-like robot ACMR5," *Proc. Int. Symp. Robot. ISR '05*, 2005.

[32] S. Takaoka, H. Yamada, and S. Hirose, "Snake-like active wheel robot ACM-R4.1 with joint torque sensor and limiter," *IEEE Int. Conf. Intell. Robot. Syst.*, pp. 1081–1086, 2011.

[33] G. Granosik, M. G. Hansen, and J. Borenstein, "The OmniTread serpentine robot for industrial inspection and surveillance," *Ind. Robot An Int. J.*, vol. 32, no. 2, pp. 139–148, 2005.

[34] J. Burgner-Kahrs, D. C. Rucker, and H. Choset, "Continuum Robots for Medical Applications: A Survey," *IEEE Trans. Robot.*, vol. 31, no. 6, pp. 1261–1280, 2015.

[35] A. Degani, H. Choset, B. Zubiate, T. Ota, and M. Zenati, "Highly Articulated Robotic Probe for Minimally Invasive Surgery," *Conf. Proc. IEEE Eng. Med. Biol. Soc.*, vol. 2006, no. 1.642343E6, pp. 4167–4172, 2006.

[36] M. G. Catalano, G. Grioli, E. Farnioli, a. Serio, C. Piazza, and a. Bicchi, "Adaptive synergies for the design and control of the Pisa/IIT SoftHand," *Int. J. Robot. Res.* , vol. 33, no. 5, pp. 768–782, 2014.

[37] R. H. Grebenstein et al, 2011. C. Grebenstein, A. Albu-Schaffer, T. Bahls, M. Chalon, O. Eiberger, W. Friedl, R. Gruber, S. Haddadin, U. Hagn, "The dlr hand arm system," *Robot. Autom.*, 2011.

[38] C. B. A. Gimenez A. Jardon, "Diseño y simulación de un actuador de rigidez variable," *An. Ing. Mec. Rev. la Asoc. Esp. Ing. Mec.*, 2012.

[39] P. Liljeback, K. Y. Pettersen, O. Stavdahl, and J. T. Gravdahl, "Compliant control of the body shape of snake robots," *Proc. - IEEE Int. Conf. Robot. Autom.*, pp. 4548–4555, 2014.

[40] G. A. Pratt and M. M. Williamson, "Series elastic actuators," *IEEE/RSJ Int. Conf. Intell. Robot. Syst. 'Human Robot Interact. Coop. Robot.*, vol. 1, no. 1524, pp. 399–406, 1995.

[41] M. Ahmed and M. M. Billah, "Smart Material-actuated Flexible Tendon-based Snake Robot," *Int. J. Adv. Robot. Syst.*, p. 1, 2016.

Copyright © 2017 ASME